Journal of Applied Polymer Science

Orientational behaviors of silk fibroin hydrogels

Daqi Chen,[1] Zhuping Yin,[1] Feng Wu,[1] Hua Fu,[1] Subhas C. Kundu,[2,3] Shenzhou Lu [1]

[1]National Engineering Laboratory for Modern Silk, College of Textile and Clothing Engineering, Soochow University, Suzhou 215123, China

[2]Department of Biotechnology, Indian Institute of Technology Kharagpur, West Bengal 721302, India

[3]3Bs Research Group, Headquarters of the European Institute of Excellence on Tissue Engineering and Regenerative Medicine, University of Minho, AvePark 4805-017, Barco Guimaraes, Portugal

Correspondence to: S. Lu (E-mail: lushenzhou@suda.edu.cn)

ABSTRACT: In this study, a novel shear-induced silk fibroin hydrogel with three-dimensional (3D) anisotropic and oriented gel skeleton/network morphology is presented. Amphipathic anionic and nontoxic sodium surfactin is blended with the silk fibroin to decrease its gelation time during the mechanical shearing process. The fibroin/surfactin blended solutions undergo a facial shearing process to accomplish a sol–gel transition within one hour. The dynamic sol–gel transition kinetic analysis, gel skeleton/network morphology, and mechanical property measurements are determined in order to visualize the fibroin/surfactin sol–gel transition during the shearing process and its resulting hydrogel. The results demonstrate that there is significant β-sheet assembly from random coil conformations in the fibroin/surfactin blended system during the facile shearing process. The silk fibroin β-sheets further transform into a fibrous large-scale aggregation with orientational and parallel arrangements to the shearing direction. The shear-induced fibroin/surfactin hydrogel exhibits notable anisotropic and oriented 3D skeleton/network morphology and a significant mechanical compressive strength in proportion to the shearing stress, compared with the control fibroin/surfactin hydrogel undergoing no shearing process. Due to its oriented gel skeleton/network structure and significantly enhanced mechanical properties, the shear-induced fibroin/surfactin gel may be suitable as a biomaterial in 3D oriented tissue regeneration, including for nerves, the cultivation of bone cells, and the repair of defects in muscle and ligament tissues. © 2017 Wiley Periodicals, Inc. J. Appl. Polym. Sci. **2017**, *134*, 45050.

KEYWORDS: biomaterials; gels; mechanical properties; structure–property relationships

Received 20 December 2016; accepted 22 February 2017
DOI: 10.1002/app.45050

INTRODUCTION

Hydrogels are polymers with a three-dimensional (3D) network structure and high water content. This supermacromolecule skeleton structure is crosslinked by a physical/chemical method. Hydrogels usually present a regular porous morphology that ranges from 100 Å to 1 μm.[1] This porous morphology absorbs and holds a large amount of water (more than 90%[2,3]. In general, hydrogels derived from natural fibroin possess excellent biocompatibility and biodegradability. The network structures within hydrogels are usually crosslinked by molecular entanglements; secondary forces including ionic, hydrogen bonding, or hydrophobic forces; and a chemical method.[4–7] Due to their fascinating mechanical properties, excellent biocompatibility, water vapor permeability, and other strengths, the hydrogels are widely used as artificial skin, drug delivery carriers, microneedle systems, thin film optics, and biological sensors.[8–13]

In recent years, silk protein fibroin (SF) from mulberry silk *Bombyx mori* has been widely explored as a promising, safe, and reliable natural biomaterial with favorable biocompatibility and biodegradability.[14–19] Mulberry silk fiber has already been used for surgical sutures for nearly a century[20] and exhibits a lower degree of allergic or immune response.[21] As a stable dynamic and unstable thermodynamic system, the aqueous regenerated fibroin solution struggles to accomplish a sol–gel transition without exterior stimuli. As a result, the transition usually takes between one to four weeks, which is not suitable for practical applications. Many physical/chemical methods are used to enhance the sol–gel transition of fibroin, including temperature increase, pH decrease, ion surroundings or solvent polarity variation, ultrasonic treatment, surfactant usage, and chemical crosslinking methods.[22–25] An amphipathic anionic surfactant can significantly enhance the fibroin sol–gel transition by interacting with the hydrophobic and hydrophilic surroundings. This results in a more unfolded/extended protein fibroin conformation that can robustly enhance the fibroin β-sheet assembly process and fibroin gelation.[26,27] The enhanced sol–gel transition kinetics with an anionic surfactant makes a regular and random

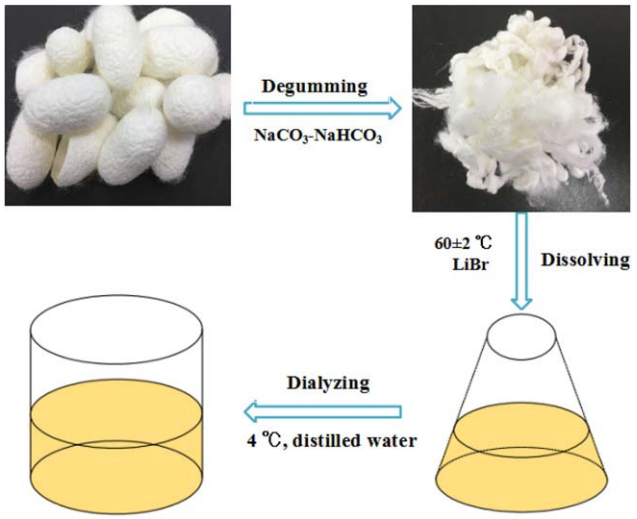

Figure 1. Preparation of regenerated silk fibroin solution. [Color figure can be viewed at wileyonlinelibrary.com]

gel network/skeleton structure. This does not require mechanical enhancement or an oriented cell culture process. The conformation of fibroin can easily transform from the random coil to β-sheet conformations during the mechanical shearing process, which results in an oriented hydrogel morphology.[28,29]

In this work, we fabricate a new shear-induced silk protein hydrogel with a 3D anisotropic and oriented gel structure/morphology by mixing or blending with fibroin and sodium surfactin (SS). This approach reduces the gelation (sol–gel transition) time of the fibroin solution. An analysis of sol–gel kinetics, gel network morphology, and mechanical properties is made during the shearing process and hydrogel formation. Hydrogel exhibits an anisotropic and oriented 3D network, as well as good mechanical properties, which may make it a suitable biomaterial for regeneration of cells usually showing oriented directional behaviors.

EXPERIMENTAL

Materials

Mulberry silk *Bombyx mori* cocoons (Suzhou Silk Treasure Biological Technology Ltd., Suzhou, China), lithium bromide (Tiancheng Chemical Co., Suzhou, China), anhydrous sodium carbonate and sodium bicarbonate (Sinopharm Chemical Reagent Co., Suzhou, China), sodium surfactin (Anhui King-Origin Biological Technology Co., Hefei, China), Slide-a-Lyzer dialysis cassettes (molecular weight cutoff = 8–10 kD, Shanghai Pouilly Biological Technology Co., Shanghai, China), and liquid nitrogen (Leshan Dongya Cryogenic Vessel Co., Leshan, China) were used for this experimentation.

Preparation of Silk Protein Fibroin Aqueous Solution and Sodium Surfactin Solution

Silk cocoons were boiled three times in a Na_2CO_3–$NaHCO_3$ (0.025–0.075 g/mL) buffer solution with a pH of 9.5. The boiled cocoons were rinsed thoroughly at least three times with deionized water (DI water) to extract the glue-like sericin proteins on the surface of the silk fibers. The degummed silks (pure silk fibers) were dried at 60 °C for at least 6 h. The pure silk fibers were then dissolved in a 9.3 *M* LiBr solution at 60 ± 2 °C for 1 h. The dissolved silk solution with approximately 15% (w/v) concentration was cooled to room temperature. The solution was dialyzed with running deionized water for 3 days using a Slide-a-Lyzer dialysis cassette. The dialyzed solution was filtered using absorbent cotton and stored at 4 °C for future use.[30] The preparation procedure of the regenerated aqueous SF solution is described in Figure 1. The 100 mg/mL sodium surfactin solution was also prepared and stored at 4 °C for future use.

Preparation of Orientational SF Hydrogels

Oriented hydrogels were obtained according to the following procedure (Figure 2). The prepared SF solution was mixed with an SS solution to obtain the SF/SS blended solution with a final SF concentration of 35 mg/mL and a final 5 mg/mL SS concentration. After the degassing process, a shearing process was applied to the aqueous SF/SS blended solution at 37 °C for 0.5 h

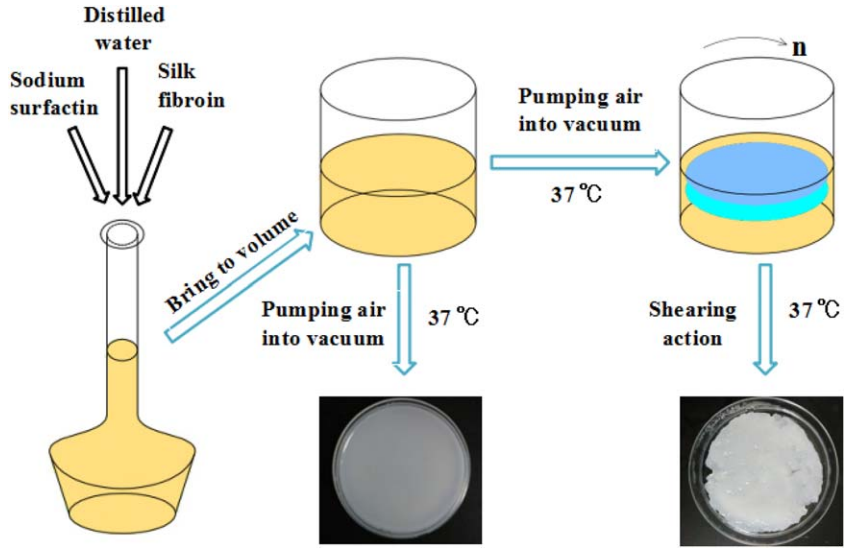

Figure 2. Fabrication of shear-induced and control SF hydrogels. [Color figure can be viewed at wileyonlinelibrary.com]

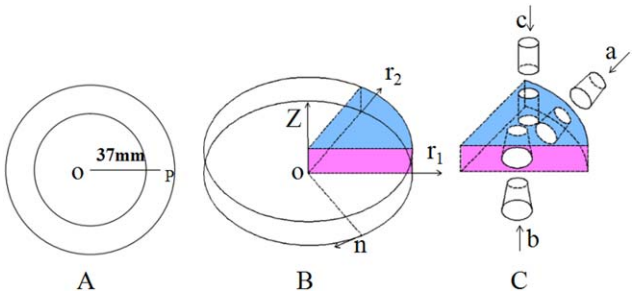

Figure 3. Model for the preparation of hydrogel samples used for SEM observations: (A) sampling location model, (B) overall model, and (C) three directions for sampling (a, b, and c). [Color figure can be viewed at wileyonlinelibrary.com]

to 1 h to obtain the shearing-induced hydrogel. Three shearing rotation speeds were set: 75 r/min, 145 r/min, and 245 r/min. The hydrogel obtained from an identical SF/SS blended solution without shearing was used as a control.

Surface Tension Measurements

The aqueous SS and SF/SS blended solutions with different SS concentrations were prepared at room temperature. The surface tension (SFT) was tested with a DataPhysics DCAT-21 (Stuttgart, Germany) surface tension instrument.[31] The speed of a precise induction lifting table was set to 1.00 mm/s for testing. The SFT values were determined when they showed a relatively stable value with a less than 0.03 mN/m difference at the last 50 instances, with three parallel samples in each group.[32]

Gelation Time Test

The aqueous SF/SS blended solutions with different SS concentrations were prepared at room temperature. The blended solution was placed in 24 well plates, each with 300 µl. They were tested with a Synergy HT microplate reader (Bio-Tek Instruments, Winooski, Vermont, US) at 37 °C with a 550 nm excitation wavelength.

Silk Fibroin Structure Change in the Gelation Process

To explore the SF conformation and aggregation structure transformation during the shearing process, the obtained silk hydrogels undergoing a shearing rotational speed of 145 r/min and with a shearing time of 0, 10, 20, 30, 40, 50, and 60 min were flash frozen in liquid nitrogen and dried in a freeze dryer. The samples were cut into fine microparticles of less than 80 µm in diameter. They were then pressed into potassium bromide (KBr) pellets and tested using a Nicolet 5700 Fourier transform infrared spectrometer (FTIR; Thermo Nicolet, Waltham, Massachusetts, US) in the wavenumber region of 400–4000 cm^{-1}. The Raman spectrum, using a laser micro-Raman spectrometer (Horiba JY, Paris, French), was also used to reveal the SF conformation transition during the shearing process, with a 400–4000 cm^{-1} wavenumber region and a scanning time of 20 s. The Raman spectra were determined by the average accumulation of two measurements. The structure of the various samples was also tested with a X Per-Pro MPD Diffractometer (PANalytical, Almelo, Netherlands) to obtain wide-angle X-ray diffraction curves (WAXD).[33] The testing conditions were Cu Kα radiation, 40 KV, and 35 mA. X-ray diffraction was measured in reflection mode at a scanning rate of 8° min^{-1} for 2θ = 5 °–45°.[34]

Fluorescence Spectroscopy

The fluorescence probe technique was performed with an Edinburgh Instrument FLS920 (Edinburgh, UK) system to visualize the dynamic transformation of the conformation of the SF during the shearing process. The shearing rotation speed was 145 r/min, and the shearing time was 0, 5, 10, 15, 20, 25, and 30 min at 37 °C. The inherent tryptophan (Trp) was used as the interior fluorescence probe with a 290 nm excitation wavelength and 300–550 nm emission wavelength range. The excitation and emission slit widths were set to 2 nm. The sample pool thickness was 1 cm.

Micromorphology Analysis of Hydrogels

There are three sampling directions, as shown in Figure 3. All of the hydrogel samples were taken in the cycle ring with a 37-mm radius [the distance between point O and point P in Figure 3(A)] from the original big cylindrical hydrogel directly resulting from the shearing process. The obtained hydrogel samples were cut into slices with a thickness of 0.5 mm along the directions of "a" (parallel to the radius), "b" (parallel to the shearing stress), and "c" (parallel to the *z* axis); see Figure 3. The control SF/SS groups were also prepared with the directions mentioned above. They were then frozen in liquid nitrogen and dried in a freeze dryer. The dried samples were all sputter-coated with gold prior to imaging under a scanning electron microscope (SEM).

The shear rate can be calculated with the following eq. (1)[35]:

$$\gamma = \frac{\pi n r}{30 d} \quad (1)$$

where γ is the shear rate (s^{-1}), *n* is the rotational speed (r/min), *r* is the radius of the disk (mm), and *d* is the gap (mm). The diagrammatic sketch is illustrated in Figure 4.

In this paper, we select four rotational speeds: 0 r/min, 75 r/min, 145 r/min, and 245 r/min. Next, by eq. (1) we calculated that the shear rate of 0 r/min is 0 s^{-1}, and the shear rate of "a", "b," and "c" are also 0 s^{-1}. The shear rate of 75 r/min is 30 s^{-1}, and the shear rate of "a," "b," and "c" is 0 s^{-1}, 30 s^{-1}, and 0 s^{-1}, respectively. The shear rate of 145 r/min is 55 s^{-1}, and the shear rate of "a," "b," and "c" is 0 s^{-1}, 55 s^{-1}, and 0 s^{-1} respectively. The shear rate of 245 r/min is 95 s^{-1}, and the shear rate of "a," "b," and "c" is 0 s^{-1}, 95 s^{-1}, and 0 s^{-1}, respectively.

Mechanical Properties and Resilience Test

The sample shear-induced SF/SS hydrogels and the control groups were formed into a cylindrical morphology using a punch to make a hole. The final samples had a size of 9 mm

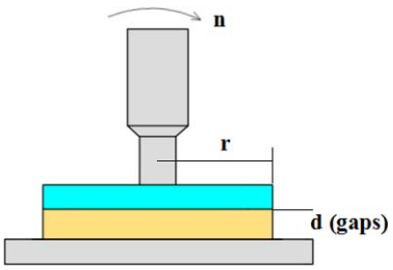

Figure 4. Diagrammatic sketch of the formula parameters. [Color figure can be viewed at wileyonlinelibrary.com]

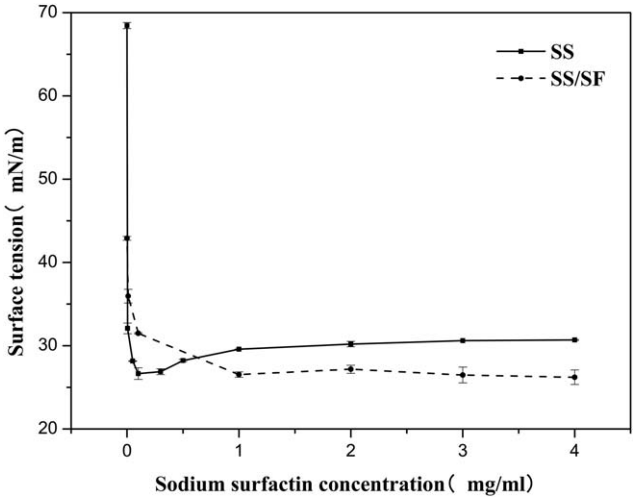

Figure 5. Surface tension of a solution. The SF concentration is 35 mg/mL in the SF/SS blended solution.

(diameter) × 9 mm (height). The hydrogel samples were then tested with a TMS-PRO TM3030 texture analyzer (Food Technology Corporation Sterling, Virginia, US) to evaluate their compressive strength, with 10 parallel samples for each group. The constant speed of compression deformation was set to 10 mm/min, and the compression ratio was 90%. The trigger force was set to 0.05 N. The compressive strength can be calculated with eq. (2):

$$\sigma_c = \frac{4 \times F}{\pi \cdot d^2} \quad (2)$$

where σ_c is the compressive strength (MPa), F is the maximum fracture load (N), and d is the diameter of the samples (mm).

Similarly, the shear-induced SF/SS hydrogels and their corresponding control groups were also measured to assess their resilience properties using the texture analyzer. The trial speed of the lift arm was 60 mm/min. The 25 mm diameter cylindrical probe was used to test with a trigger force of 0.05 N, and its detection accuracy was more than 0.015% under 40% compression. The stress–strain curves were analyzed to obtain relevant parameters for calculating the hydrogel resilience, with six parallel samples for each group. The elastic recovery rate is calculated with eq. (3):

$$r = \frac{L_2}{L_1} \times 100\% \quad (3)$$

where L_1 is the compression displacement (mm), L_2 is the resistance displacement (mm), and r is the elastic recovery rate (%).

RESULTS AND DISCUSSION

Surface Tension

Surfactants can reduce the surface tension of water. The critical micelle concentration (CMC) is the concentration of a surfactant that results in the lowest liquid surface tension.[36] This experiment reveals the relationship between the liquid surface tension and its corresponding solute concentration (Figure 5). The surface tension of pure water is approximately 70 mN/m at 37 °C, which is similar to the previously reported value.[37] When adding the sodium surfactin to water, the surface tension of pure water decreases rapidly, and the CMC is approximately 0.005–0.1 mg/mL. We also found that the increase of the sodium surfactin (SS) concentration led to a robust decrease of its surface tension until reaching the CMC. Sodium surfactin is a kind of amphiphilic biological macromolecule that tends to gather in the interface of two different phases and form an interface layer. This special layer makes the surface of the water solution into the interface of the hydrophobic groups and air, and thus the surface tension of water shows a sharp drop.[38] This point is less than the CMC. The surface tension decreases, and then the slope of the curve begins to rise to a stable value, due to the increase of the ion concentration making the countra-ions gather in the solution and form the micelle.[39] For the silk fibroin/sodium surfactin (SF/SS) blended solution, the surface tension reduces rapidly at 0.1 mg/mL and remains at a stable value when the SS concentration reaches its CMC. As the concentration of sodium surfactin further increases, the charged interaction is also enhanced. It is easy for silk fibroin molecules to assemble into advanced structures, and the solution is transformed into a precipitate and then eventually into a gel.[40–42]

Gelation Time of Silk Fibroin/Sodium Surfactin Solution

An SF solution is mixed with an SS solution until the final SF concentration is 35 mg/mL, and the final SS concentrations are 0, 1, 2, 3 and 4 mg/mL (Table I). The results show that the pure SF solution cannot gel within 24 h, and the sol–gel transition is extremely difficult due to a stable dynamic and unstable thermodynamic system and usually takes between a week and a month for the gelation to occur.[43] When the SS concentration increases to 1 mg/mL, the gelation time is shortened rapidly, and a further increase of the SS generates a reduction in its gelation time. Based on the relationship between the surface tension and SS concentration, we found a decrease of its surface tension, which lead to the reduction of its gelation time. When imposing shear action, there is a shorter gelation time due to enhancing the SF sol–gel transition kinetics, in comparison with the conformation transition without shear processes.

SF Conformation Changes in the Gelation Process

To determine why the aqueous SF/SS blended solution undergoing a shearing process can easily make a flowing sol to a robust

Table I. Gel Time of Blended Solution in Different SS Concentrations

SS (mg/mL)	Conditions	Gel time (h)	Gel state
0	no shearing	>24 h	ungelled
	shearing	>24 h	ungelled
1	no shearing	6 h	gelled
	shearing	~5 h	gelled
2	no shearing	4.5 h	gelled
	shearing	~3 h	gelled
3	no shearing	2.5 h	gelled
	shearing	~2 h	gelled
4	no shearing	1.5 h	gelled
	shearing	~0.75 h	gelled

The final SF concentration is 35 mg/mL, and the shearing rotation speed is 145 r/min.

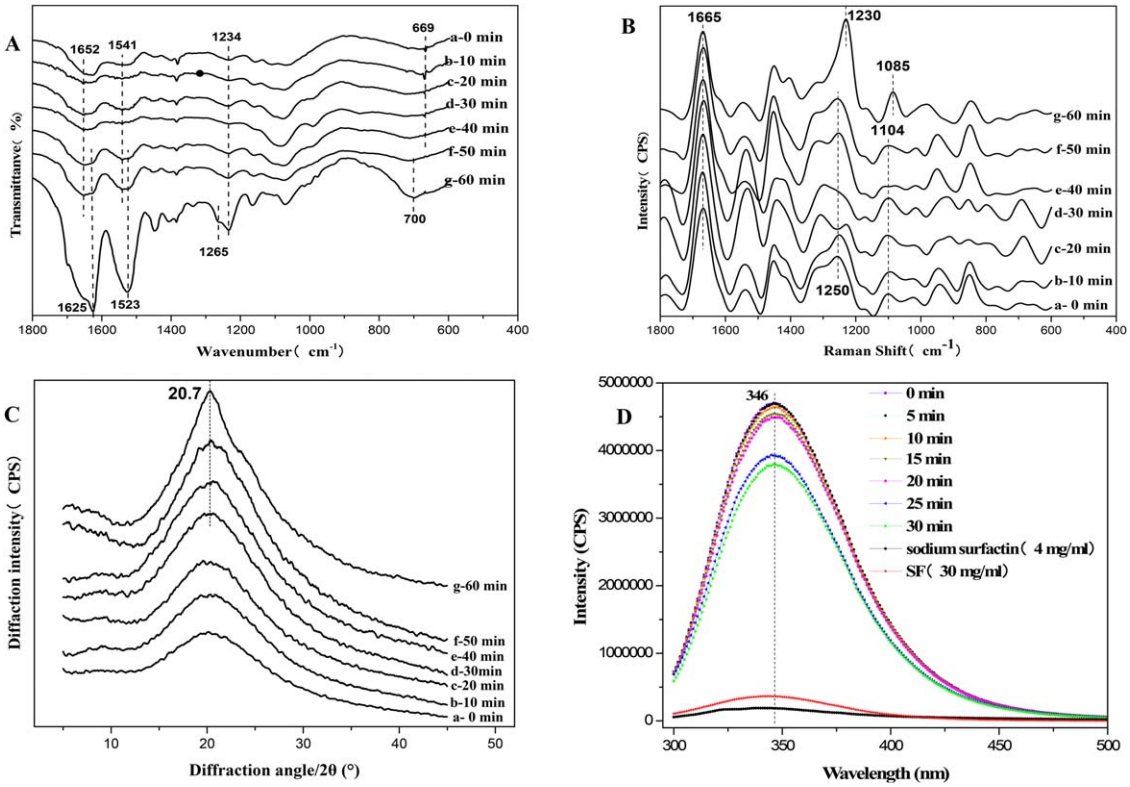

Figure 6. SF structure change during shearing: (A) FTIR; (B) Raman spectra; (C) XRD; (D) fluorescent emission spectra. Concentrations of SF and SS are 35 mg/mL and 5 mg/mL, respectively. The shearing rotation speed is 145 r/min. [Color figure can be viewed at wileyonlinelibrary.com]

gel transition, the FTIR, Raman, and X-ray diffraction spectra were used to measure their changing microstructures during the shearing process. The results demonstrate that there is a significant conformational transformation from random coil to β-sheet conformations in the SF/SS blended system during its shearing process. This finding corresponds to an amorphous aggregation structure in a typical silk II crystal structure transformation and a remarkably enhanced sol–gel transition [Figure 6(A–C)]. The SF/SS blended groups undergoing the shearing process for 0–50 min exhibit infrared absorption peaks at 1652 cm^{-1} (amide I) and 1541 cm^{-1} (amide II) and Raman scattering peaks at 1665 cm^{-1} (amide I), 1250 cm^{-1} (amide III), and 1104 cm^{-1} (C—C), with a relatively broad peak in the XRD curves and a flowing characteristic. This indicates that the SF/SS blended system shows a typical random coil conformation and an amorphous aggregation structure during its initial shearing process for 0–50 min.[44] In contrast, the SF/SS blended system undergoes a 60-min shearing process, and sharp infrared absorption peaks are found at 1625 cm^{-1} (amide I), 1523 cm^{-1} (amide II), and 1265 cm^{-1} (amide III), and Raman peaks are found at 1665 cm^{-1} (amide I), 1230 cm^{-1} (amide III), and 1085 cm^{-1} (C—C), with an extremely sharp peak at 20.7° in the XRD curve. These are the characteristics of β-sheet conformations and a representative silk II crystal structure.[44] Meanwhile, the aqueous SF/SS blended solution underwent a complete sol–gel transition within the shearing time of 50–60 min. The results indicate that the SF/SS blended solution can easily accomplish a β-sheet conformation and a representative silk II crystal structure during the facile mechanical shearing procedure in a relatively short time, usually 1 h. The identical conformation transition usually occurs in a pure aqueous SF solution in between one week and one month.

Fluorescent Spectra Analysis

Fluorescent probe technology has drawn much attention and been widely explored due to its extremely sensitive and dynamic emissions resulting from the microchanges in the liquid surrounding it, with no damage to the samples being detected. Trp is the inherent fluorescent amide that exists in SF, which is thus used as the interior fluorescent probe to monitor the changing microstructure in the SF/SS blended system during the shearing process.

The results indicate that the initial aqueous SF/SS blended solution shows significantly higher emission intensity at the position of 346 nm than the pure aqueous SF solution at the same concentration [Figure 6(D)]. This finding is due to more extended/unfolded SF molecular chains and a more exposed situation for Trp in water due to the influence of the amphipathic SS.[45] However, there is a remarkable decrease in fluorescent intensity of the SF/SS blended system during its shearing process. This may due to β-sheet aggregations, which lead to an unexposed situation for the Trp amide. This agrees well with the results mentioned above [Figure 6(A–C)]. The enhanced sol–gel of the SF/SS blended solution is indeed a β-sheet assembling process, which makes the final SF/SS gel skeleton structure.

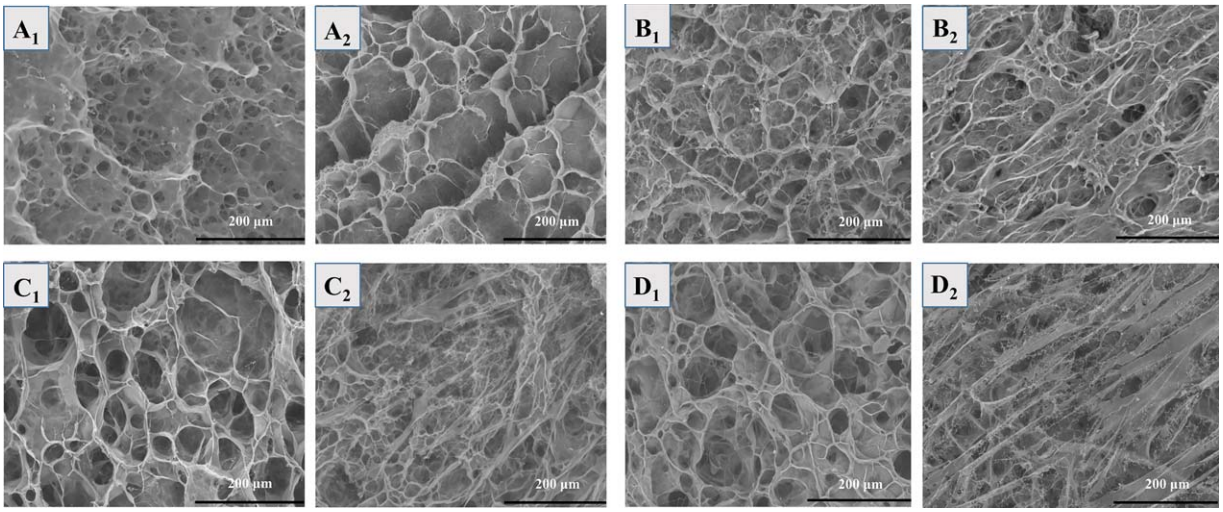

Figure 7. Morphologies of the hydrogels under SEM: (A_1) cross sections of silk fibroin/sodium surfactin (SF/SS hydrogels without shearing process); (A_2) vertical section of SF/SS hydrogels without shearing process. (B_1) and (B_2) are the morphological images of the surface, perpendicular to "a" and perpendicular to "c," of the hydrogels. They are sampled 37 mm away from the circle center prepared using a shearing rotation speed of 75 r/min. (C_1) and (C_2) are the images perpendicular to "a" and perpendicular to "c" of the hydrogels prepared at 145 r/min. (D_1) and (D_2) are the images perpendicular to "a" and perpendicular to "c" of the hydrogels prepared at 245 r/min. The concentrations of SF and SS are 35 mg/mL and 5 mg/mL, respectively. [Color figure can be viewed at wileyonlinelibrary.com]

Morphological Observations of the Hydrogels under Scanning Electron Microscopy

The SEM observations are used to measure the skeleton/network structure of freeze-dried SF/SS hydrogel under different levels of shearing stress. The control SF/SS groups undergoing no shearing processes exhibit a normal and isotropic 50–100 μm 3D porous morphology both inside and outside the gel [Figure 7(A_1,A_2)]. The shear-induced SF/SS hydrogels perpendicular to the direction of shearing stress have a regular porous morphology, and there is no obviously oriented gel skeleton/network structure with various shearing stresses [Figure 7(B_1,C_1,D_1)]. However, the shear-induced SF/SS hydrogels parallel to the direction of shearing stress show an oriented gel skeleton/network structure in proportion to its shearing stress [Figure 7(B_2,C_2,D_2)]. This is compared with the irregular porous morphology in the control SF/SS gel. The shear-induced SF/SS gel sampled perpendicular to the shearing stress shows an irregular 3D porous morphology, similar to the skeleton/network structure in the control SF/SS gel. Thus, the shear-induced SF/SS hydrogel is indeed an anisotropic system. The higher the shearing stress, the more oriented the skeleton/network structure, and the larger and thicker the fibrous SF aggregations parallel to its corresponding shearing stress. The results demonstrate that the shearing process during the SF/SS gelation can make the SF β-sheets further assemble into large-scale fibrous aggregations arranged parallel to the shearing stress. This effect creates the final anisotropic and oriented SF gel skeleton/network. The shearing process makes the protein molecular chains stretch along the axial direction and generates a continuous orientational network structure, resulting in the discontinuous fibrous crystal structure, and thereby the crystal structure orientation is consistent with the shearing stress.[46] There is no obvious orientation structure in the direction of zero shear force. Under lower shearing stress, no obvious fibrous crystal morphology occurs, mainly because of its inability to make a fibrous crystal precursor in a low shearing field.[47,48] With the increase of shearing stress, the orientational fiber crystal morphology becomes clear. It is believed that the fibrous crystal structures are made up of long tensile chains caused by the shearing force.[49,50]

Mechanical Properties and Resilience Performance

A texture analyzer is used to measure and evaluate the mechanical difference between the shear-induced and control SF/SS hydrogel. Notably, the shear-induced SF/SS hydrogel holds a higher compressive strength and modulus than the control SF/SS group in all of their sampling directions (Figure 8 and Figure 9). The shear-induced hydrogels undergoing different shearing rates and sampled in all directions (directions "a," "b," and "c") as mentioned above show a remarkably higher compressive strength than their corresponding control isotropic gel at identical SF/SS concentrations. Moreover, the shear-induced hydrogels sampled in direction "b" and undergoing different shearing rates show a higher compressive strength than their corresponding gels sampled in directions "a" and "c." This is in accordance with the direction of the shearing stress and the direction of the arranged large-scale fibrous β-sheet aggregations in the shear-induced anisotropic gel skeleton/network. The higher the shearing rate, the stronger the mechanical properties of the shear-induced SF/SS gels are in all sampling directions. A comparison of the SEM images and the experimental results indicates that the silk fibroin molecular chains are extended by the constant shearing rate and that the molecular chains slip and arrange along the drawing direction. This forms an oriented fibrous crystallization structure, which probably improves the mechanical properties of the hydrogels.[51] There is no obvious difference

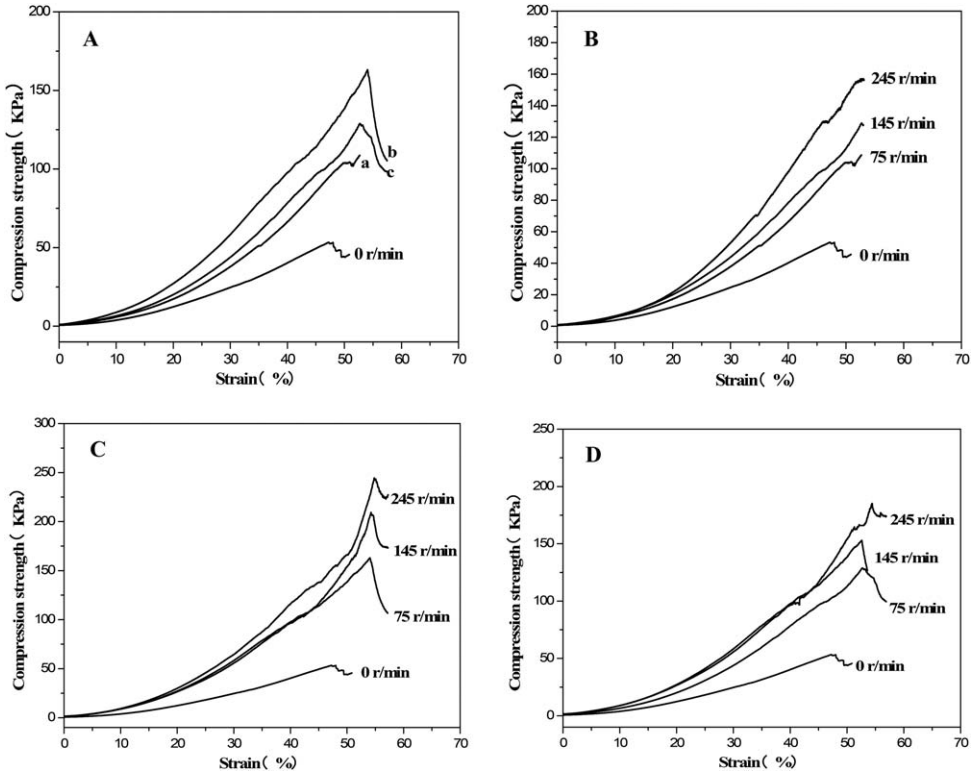

Figure 8. Compression strength–strain curves: (A) shearing rotation speed of 75 r/min; (B) direction "a," (C) direction "b," and (D) direction "c." The concentrations of SF and SS are 35 mg/mL and 5 mg/mL, respectively.

in fracture strain and elastic recovery among the shear-induced SF/SS gels sampled in all directions ("a," "b," and "c") and the control group, regardless of the shearing stress (Figure 9 and Figure 10). The greater orientation may lead to stress lagging and improve the elastic performance. The results indicate that the anisotropic and oriented gel skeleton/network structure resulting from a shearing process can make a stronger SF/SS gel compared with the normal isotropic version. A higher shearing rate accomplishes a more remarkable oriented gel skeleton/network structure and thus results in a stronger SF gel.

CONCLUSIONS

The blended silk fibroin/sodium surfactin solution can accomplish a thorough sol–gel transition within one hour during a facial mechanical shearing process. The shear-induced SF/SS hydrogels exhibit an anisotropic and oriented gel skeleton/network morphology, in which the oriented direction is parallel to its corresponding shearing stress. The higher the shearing stress is, the more remarkable the oriented gel skeleton/network morphology is, and the tougher the SF/SS gels are. The compressive strength and modulus of the shear-induced hydrogel sampled in the direction parallel to the shearing stress is significantly larger than those sampled in any other direction. The anisotropic, oriented β-sheet structure and the mechanical strength of the shear-induced SF/SS hydrogel make it acceptable as a biomaterial for applications in 3D oriented tissue regeneration, such as in nerves, cultivation of bone cells, and repair of defects in muscle and ligament tissues.

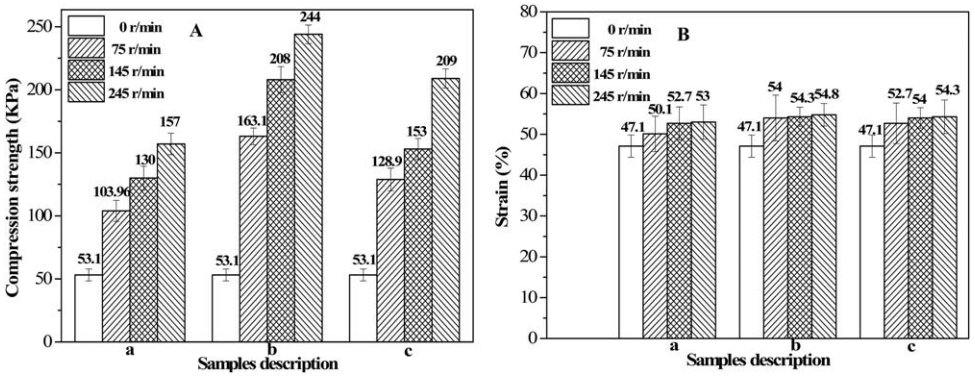

Figure 9. Compressive mechanical properties of samples: (A) average compression strength of samples; (B) average compression strain of samples. The concentrations of SF and SS are 35 mg/mL and 5 mg/mL, respectively ($n = 4$).

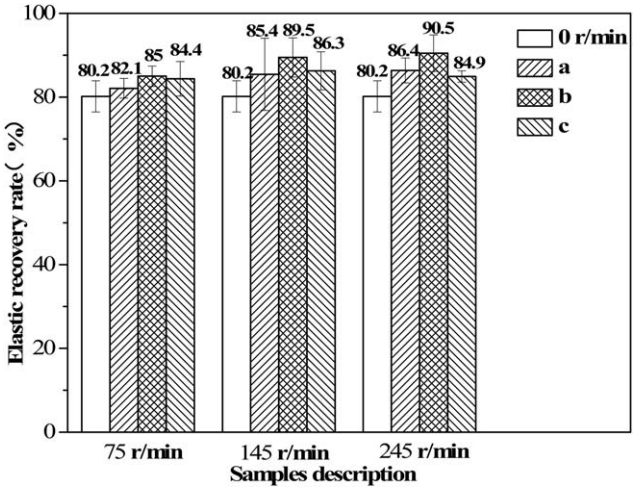

Figure 10. Average elastic recovery rate under different shearing stresses ($n = 4$).

ACKNOWLEDGMENTS

The work is supported by National Natural Science Foundation of China (Grant No. 51373114), PAPD and College Nature Science Research Project of Jiangsu Province, China (Grant No. 15KJA540001). S. C. Kundu holds ERA Chair Full Professor of European Commission Programme (RoReCaST) at 3Bs Research Group, University of Minho, Portugal.

REFERENCES

1. Amin, S.; Rajabnezhad, S.; Kohli, K. *Sci. Res. Ess.* **2009**, *4*, 1175.
2. Numata, K.; Katashima, T.; Sakai, T. *Biomacromolecules* **2011**, *12*, 2137.
3. Peppas, N. A.; Bures, P.; Leobandung, W.; Ichikawa, H. *Eur. J. Pharm. Biopharm.* **2000**, *50*, 27.
4. Johnson, J. A.; Turro, N. J.; Koberstein, J. T.; Make, J. E. *Prog. Polym. Sci.* **2010**, *35*, 332.
5. Hennink, W. E.; Nostrum, N. J. C. F. V. *Adv. Drug Deliv. Rev.* **2012**, *64*, 223.
6. Lin, S. J.; Schattling, P.; Theato, P. *Sci. Adv. Mater.* **2015**, *7*, 948.
7. Mengge, X.; Cheng, Y. H.; Meng, Z. Q.; Jiang, X. Z.; Chen, Z. G.; Patrick, T.; Zhu, M. F. *Macromol. Rapid Commun. Sci.* **2015**, *36*, 477.
8. Drury, J. L.; Mooney, D. *J. Biomater.* **2003**, *24*, 4337.
9. Zhang, Y.; Zhu, W.; Wang, B.; Ding, J. *J. Control. Release* **2005**, *105*, 260.
10. Graeter, S. V.; Huang, J.; Perschmann, N.; Lopez-Garcia, M.; Kessler, H.; Ding, J.; Spatz, J. P. *Nano Lett.* **2007**, *7*, 1413.
11. Lee, K. Y.; Mooney, D. *J. Chem. Rev.* **2001**, *101*, 1869.
12. Hoffman, A. S. *Adv. Drug Deliv. Rev.* **2002**, *54*, 3.
13. Rudzinski, W. E.; Dave, A. M.; Vaishnav, U. H.; Kumbar, S. G.; Kulkarni, A. R.; Aminabhavi, T. M. *Des. Monomers Polym.* **2002**, *5*, 39.
14. Rajkhowa, R.; Levin, B.; Redmond, S. L.; Li, L. H.; Wang, L. J.; Kanwar, J. R.; Atlas. M. D.; Wang, X. G. *J. Biomed. Mater. Res.* **2011**, *97*, 37.
15. Zhao, H. S.; Heusler, E.; Jones, G.; Li, L. H.; Werner, V.; Germershaus, O.; Ritzer, J.; Luehmann, T.; Meinel, L. *Sruct. Biol.* **2014**, *186*, 420.
16. Kundu, S. C.; Kundu, B.; Talukdar, S.; Bano, S.; Nayak, S.; Kundu, J.; Mandal, B. B.; Bhardwaj, N.; Botlagunta, M.; Dash, B. C.; Acharya, C.; Ghosh, A. K. *Biopolym.* **2012**, *97*, 455.
17. Kundu, B.; Rajkhowa, R.; Kundu, S. C.; Wang, X. *Adv. Drug Deliv. Rev.* **2013**, *65*, 457.
18. Kapoor, S.; Kundu, S. C. *Acta Biomater.* **2016**, *31*, 17.
19. Kundu, B.; Kurland, N. E.; Subia, B.; Patra, C.; Engel, F. B.; Yadavalli, V. K.; Kundu, S. C. *Prog. Polym. Sci.* **2014**, *39*, 251.
20. Vepari, C.; Kaplan, D. L. *Prog. Polym. Sci.* **2007**, *32*, 991.
21. Grace Chao, P.-H.; Yodmuang, S.; Wang, X.; Sun, L.; Kaplan, D. L.; Gordana, V.-H. *J. Biomed. Mater. Res. B: Appl. Biomater.* **2010**, *95*, 84.
22. Foo, C. W. P.; Bini, E.; Hensman, J.; Knight, D. P.; Lewis, R. V.; Kaplan, D. L. *Appl. Phys. A Mater. Sci. Process.* **2006**, *28*, 223.
23. Hu, X.; Lu, Q.; Sun, L.; Cebe, P.; Wang, X. Q.; Zhang, X. H.; Kaplan, D. L. *Biomacromolecules* **2010**, *11*, 3178.
24. Nagarkar, S.; Nicolai, T.; Chassenieux, C.; Lele, A. *Phys. Chem. Chem. Phys.* **2010**, *12*, 3834.
25. Li, X. G.; Wu, L. Y.; Huang, M. R.; Shao, H. L.; Hu, X. C. *Biopolym.* **2008**, *89*, 497.
26. Wang, X. Q.; Kluge, J. A.; Leisk, G. G.; Kaplan, D. L. *Biomater.* **2008**, *29*, 1054.
27. Wu, X. L.; Hou, J.; Li, M. Z.; Wang, J. N.; Kaplan, D. L.; Lu, S. Z. *Acta Biomater.* **2012**, *8*, 2185.
28. Fini, M.; Motta, A.; Torricelli, P.; Giavaresi, G.; Aldini, N. N.; Tschon, M.; Giardino, R.; Migliaresi, C. *Biomater.* **2005**, *26*, 3527.
29. Motta, A.; Migliaresi, C.; Faccioni, F.; Torricelli, P.; Fini, M.; Giardino, R. *J. Biomater. Sci.* **2004**, *15*, 851.
30. Roehl, D.; Jelen, P. *J. Dairy Sci.* **1988**, *71*, 3167.
31. Rosen, M. J.; Cohen, A. W.; Dahanayake, M.; Hua, X. Y. *J. Phys. Chem.* **1982**, *86*, 541.
32. Kim, U. J.; Park, J.; Li, C.; Jin, H. J.; Valluzzi, R.; Kaplan, D. L. *Biomacromolecules* **2004**, *5*, 786.
33. Zhong, T. Y.; Deng, C. M.; Gao, Y. F.; Chen, M.; Zuo, B. Q. *J. Biomed. Mater. Res. Part A* **2012**, *100*, 1983.
34. Silva, S. S.; Popa, E. G.; Gomes, M. E.; Oliveira, M. B.; Nayak, S.; Subia, B.; Mano, J. F.; Kundu, S. S.; Reis, R. L. *Acta Biomater.* **2013**, *9*, 8972.
35. Metzner, A. B.; Otto, R. E. *AIChE J.* **1959**, *3*, 3.
36. Rosen, M. J.; Mathias, J. H.; Davenport, L. *Langmuir* **1999**, *15*, 7340.
37. Pallas, N. R.; Harrison, Y. *Colloid Surf.* **1963**, *1*, 367.
38. Yu, Z. J.; Zhang, X. K.; Xu, G. Z.; Zhao, G. X. *J. Phys. Chem.* **1990**, *94*, 3675.
39. Sun, C. Y.; Chen, G. J.; Yang, L. Y. *J. Chem. Eng. Data.* **2004**, *49*, 1023.
40. Morn, A. K.; Khan, A. *J. Colloid Interface Sci.* **1999**, *218*, 397.
41. Yamaura, K.; Okumura, Y.; Ozaki, A.; Matsuzawa, S. *J. Appl. Polym. Sci.* **1985**, *41*. 205.

42. Morn, A. K.; Nydn, M.; Derman, O. S. *Langmuir* **1999**, *15*, 5480.
43. Morn, A. K.; Regev, O.; Khan, A. *J. Colloid Interface Sci.* **2000**, *222*, 170.
44. Matsumoto, A.; Chen, J. S.; Collette, A. L.; Kim, U. J.; Altman, H. A.; Cebe, P.; Kaplan, D. L. *J. Phys. Chem. B.* **2006**, *110*, 21630.
45. Zainuddin; Le, T. T.; Park, Y.; Chirila, T. V.; Halley, P. J.; Whittaker, A. K. *Biomater.* **2008**, *29*, 4268.
46. Park, S. H.; Cho, H.; Gil, E. S.; Mandal, B. B.; Min, B. Y.; Kaplan, D. L. *Tissue Eng. Part A* **2011**, *17*, 2999.
47. Wen, H. Y.; Jiang, S. C.; Men, Y.; Zhang, X. Q.; An, L. J.; Wu, Z. H.; Okuda, H. *J. Chem. Phys.* **2009**, *130*, 164909-1.
48. Kielhorn, L.; Colby, R. H.; Han, C. C. *Macromolecules* **2000**, *33*, 2486.
49. Han, C. C.; Yao, Y. H.; Zhang, R. Y.; Hobbie, E. K. *Polymer* **2006**, *47*, 3271.
50. Seki, M.; Thurman, D. W.; Oberhauser, J. P.; Kornfield, J. A. *Macromolecules* **2002**, *35*, 2583.
51. Zhang, X. M.; Li, X. L.; Wang, D. M.; Yin, Z. H. *J. Appl. Polym. Sci.* **1997**, *64*, 1489.